

Centrality dependence of global variables in relativistic heavy ion collisions: Final p_T data analysis in the framework of a statistical model

Dariusz Prorok*

*Institute of Theoretical Physics, University of Wrocław,
Pl. Maksa Borna 9, 50-204 Wrocław, Poland*

(Dated: April 19, 2006)

The global variables like the transverse energy at midrapidity, the charged particle multiplicity at midrapidity and the total multiplicity of charged particles are evaluated in the single-freeze-out statistical model for different centrality bins at RHIC at $\sqrt{s_{NN}} = 130$ and 200 GeV. Full description of decays of hadron resonances is applied in these estimations. The geometric parameters of the model are obtained from the fit to the final data on the p_T spectra. The predicted values of the global variables agree qualitatively well with the experimental data. The centrality independence of the total number of charged particles per participant pair has been also reproduced.

PACS numbers: 25.75.-q, 25.75.Dw, 24.10.Pa, 24.10.Jv

I. INTRODUCTION

In the previous paper [1] the extensive analysis of the centrality dependence of two measured global variables, transverse energy ($dE_T/d\eta|_{mid}$) and charged particle multiplicity ($dN_{ch}/d\eta|_{mid}$) densities at mid-rapidity as well as their ratio, was delivered. The analysis was done in the framework of the single freeze-out statistical model [2, 3, 4] for the Au-Au collisions at RHIC at $\sqrt{s_{NN}} = 130$ and 200 GeV. The main idea of this method is as follows. Thermal and geometric parameters of the model are established from fits to particle yield ratios and p_T spectra, respectively. Then, with the use of these parameters both densities $dE_T/d\eta$ and $dN_{ch}/d\eta$ as well as the total charged-particle multiplicity can be estimated and compared with the data. The main reason for doing it is that the transverse energy and charged particle multiplicity measurements are independent of hadron spectroscopy (in particular, no particle identification is necessary), therefore they could be used as an additional test of the self-consistency of a statistical model. In the present paper the above-mentioned program will be performed once more for the reasons stated below.

First of all fits of the geometric parameters [5] were done with the use of the preliminary data for the p_T spectra measured at RHIC at $\sqrt{s_{NN}} = 200$ GeV [6, 7]. But the final data [8, 9] differ substantially from the preliminary ones. Additionally the data points for the χ^2 analysis were digitized from the plots. Also not all centrality bins were fitted in [5, 10]. All of these resulted in the rough qualitative agreement of the model predictions for $dN_{ch}/d\eta$ and $dE_T/d\eta$ for RHIC at $\sqrt{s_{NN}} = 200$ GeV [1]. And the centrality independence of the total multiplicity of charged particles per participant pair was not reproduced. The evidence for such scaling of the total multiplicity was reported by the PHOBOS Collaboration [11]. Therefore it was very tempting to check whether the χ^2 analysis of the final data for the p_T spectra of identified charged hadrons would improve the predictions for transverse energy and charged particle multiplicity densities and the total charged-particle multiplicity. Such a check is *nontrivial* and *does not mean* simply adding the integrals of the experimental momentum distributions because: (a) spectra are measured in the limited ranges of p_T and the very important low- p_T part is not detected, (b) spectra of stable neutral particles like neutrons and K_L^0 are not measured generally.

As a statistical model the single freeze-out model is taken (for details see [10]). The model succeeded in the accurate description of ratios and p_T spectra of particles measured at RHIC [2, 3, 4]. The main postulate of the model is the simultaneous occurrence of chemical and thermal freeze-outs, which means that the possible elastic interactions after the chemical freeze-out are neglected. The conditions for the freeze-out are expressed by values of two independent thermal parameters: T and μ_B . The strangeness chemical potential μ_S is determined from the requirement that the overall strangeness equals zero. The second basic feature of the model is the complete treatment of resonance decays. This means that the final distribution of a given particle consists not only of the thermal part but also of contributions from all possible decays and cascades. Feeding from weak decays is included as well.

*Electronic address: prorok@ift.uni.wroc.pl

II. THE FOUNDATIONS OF THE SINGLE-FREEZE-OUT MODEL

The main assumptions of the model are as follows: (a) the chemical and thermal freeze-outs take place simultaneously, (b) all confirmed resonances up to a mass of 2 GeV from the Particle Data Tables [12] are taken into account, (c) a freeze-out hypersurface is defined by the equation

$$\tau = \sqrt{t^2 - r_x^2 - r_y^2 - r_z^2} = \text{const} , \quad (1)$$

(d) the four-velocity of an element of the freeze-out hypersurface is proportional to its coordinate

$$u^\mu = \frac{x^\mu}{\tau} = \frac{t}{\tau} \left(1, \frac{r_x}{t}, \frac{r_y}{t}, \frac{r_z}{t} \right) , \quad (2)$$

(e) the following parameterization of the hypersurface is chosen:

$$t = \tau \cosh \alpha_{\parallel} \cosh \alpha_{\perp}, \quad r_x = \tau \sinh \alpha_{\perp} \cos \phi, \quad r_y = \tau \sinh \alpha_{\perp} \sin \phi, \quad r_z = \tau \sinh \alpha_{\parallel} \cosh \alpha_{\perp}, \quad (3)$$

where α_{\parallel} is the rapidity of the element, $\alpha_{\parallel} = \tanh^{-1}(r_z/t)$, and α_{\perp} controls the transverse radius:

$$\rho = \sqrt{r_x^2 + r_y^2} = \tau \sinh \alpha_{\perp} < \rho_{\text{max}} , \quad (4)$$

where the restriction on the transverse size has been introduced, so ρ_{max} gives the maximal transverse extension of the gas in the central slice during the freeze-out. This means that two new parameters of the model have been introduced, *i.e.* τ and ρ_{max} , which are connected with the geometry of the freeze-out hypersurface. In general a freeze-out addresses a 6-dimensional phase-space but the assumption of the Hubble-like expansion (the velocity at the freeze-out is proportional to the coordinate), Eq. (2), reduces the number of independent variables to 3. And the assumption of the cylindrical symmetry further reduces this number to 2. Another point is how realistic the assumption of the Hubble flow is. Recent results of Refs. [13, 14] indicate that the Hubble flow of the form of Eq. (2) can develop in 130 and 200 GeV Au-Au collisions within times 6-15 fm. This is roughly the scale of the freeze-out initializing time predicted in this analysis for all but peripheral bins (see Table I).

From Eq. (1) one can see that the beginning of the freeze-out process starts at $t_{f.o.}^{(1)} = \tau$ and $\vec{r} = 0$ in the c.m.s., which is also the laboratory frame in the RHIC case. At this moment the volume of the gas can be estimated as

$$V_{f.o.}^{(1)} = 2\pi\tau\rho_{\text{max}}^2 , \quad (5)$$

which is simply the volume of a tube with a length 2τ and a radius ρ_{max} (2τ is the maximal possible extension of the gas in the longitudinal direction at $t_{f.o.}^{(1)}$). In the central slice the freeze-out ceases at $t_{f.o.}^{(2)} = \sqrt{\tau^2 + \rho_{\text{max}}^2}$ and it takes place at $\rho = \rho_{\text{max}}$. This *does not mean* the end of the freeze-out process completely. It is the moment when the gas decouples into two pieces symmetrical with respect to the plane $z = 0$ and from then the freeze-out proceeds into two opposite directions of the collision axis z . For the considered hypersurface, Eq. (1), this process extends to infinity but to be more realistic a limiting condition for α_{\parallel} will be assumed in Sec. IV C, namely a maximal possible value of α_{\parallel} called $\alpha_{\parallel}^{\text{max}}$ will be postulated. Then the moment when the freeze-out ceases at all will be equal to

$$t_{f.o.}^{(3)} = \cosh \alpha_{\parallel}^{\text{max}} \cdot t_{f.o.}^{(2)} . \quad (6)$$

At $t_{f.o.}^{(2)}$ the volume of the region where the freeze-out process has just taken place or is to happen can be estimated as

$$V_{f.o.}^{(2)} = 2\pi\sqrt{\tau^2 + \rho_{\text{max}}^2} \rho_{\text{max}}^2 . \quad (7)$$

The transverse velocity in the central slice can be expressed as a function of the transverse radius

$$\beta_{\perp}(\rho) = \tanh \alpha_{\perp} = \frac{\rho}{\sqrt{\tau^2 + \rho^2}} . \quad (8)$$

The maximum value of β_{\perp} called the maximum transverse-flow parameter (or the surface velocity) is given by

$$\beta_{\perp}^{max} = \frac{\rho_{max}}{\sqrt{\tau^2 + \rho_{max}^2}} = \frac{\rho_{max}/\tau}{\sqrt{1 + (\rho_{max}/\tau)^2}}. \quad (9)$$

The invariant distribution of the measured particles of species i has the form [3, 4]

$$\frac{dN_i}{d^2p_T dy} = \int p^{\mu} d\sigma_{\mu} f_i(p \cdot u), \quad (10)$$

where $d\sigma_{\mu}$ is the normal vector on a freeze-out hypersurface, $p \cdot u = p^{\mu} u_{\mu}$, u_{μ} is the four-velocity of a fluid element and f_i is the final momentum distribution of the particle in question. The final distribution means here that f_i is the sum of primordial and simple and sequential decay contributions to the particle distribution (for details see [10, 15]).

With the use of Eqs. (2) and (3), the invariant distribution (10) takes the following form:

$$\frac{dN_i}{d^2p_T dy} = \tau^3 \int_{-\infty}^{+\infty} d\alpha_{\parallel} \int_0^{\rho_{max}/\tau} \sinh \alpha_{\perp} d(\sinh \alpha_{\perp}) \int_0^{2\pi} d\xi (p \cdot u) f_i(p \cdot u), \quad (11)$$

where

$$p \cdot u = m_T \cosh(\alpha_{\parallel} - y) \cosh \alpha_{\perp} - p_T \cos \xi \sinh \alpha_{\perp}. \quad (12)$$

After changing the integration variable α_{\parallel} to $\alpha_{\parallel} + y$ the invariant distribution (11) still has the same form but with $p \cdot u$ replaced now by $\widetilde{p \cdot u}$:

$$\widetilde{p \cdot u} = m_T \cosh \alpha_{\parallel} \cosh \alpha_{\perp} - p_T \cos \xi \sinh \alpha_{\perp}. \quad (13)$$

That was for the case of unlimited α_{\parallel} . If α_{\parallel} is limited and has its maximal value α_{\parallel}^{max} then the invariant distribution (10) reads

$$\frac{dN_i}{d^2p_T dy} = \tau^3 \int_{-\alpha_{\parallel}^{max}}^{\alpha_{\parallel}^{max}} d\alpha_{\parallel} \int_0^{\rho_{max}/\tau} \sinh \alpha_{\perp} d(\sinh \alpha_{\perp}) \int_0^{2\pi} d\xi (p \cdot u) f_i(p \cdot u) = \int d\sigma (p \cdot u) f_i(p \cdot u). \quad (14)$$

The same changing of the integration variable $\alpha_{\parallel} \rightarrow \alpha_{\parallel} + y$ can be done and one obtains

$$\frac{dN_i}{d^2p_T dy} = \tau^3 \int_{-\alpha_{\parallel}^{max}-y}^{\alpha_{\parallel}^{max}-y} d\alpha_{\parallel} \int_0^{\rho_{max}/\tau} \sinh \alpha_{\perp} d(\sinh \alpha_{\perp}) \int_0^{2\pi} d\xi (\widetilde{p \cdot u}) f_i(\widetilde{p \cdot u}). \quad (15)$$

The distribution (15) is still boost invariant because rapidity differences are invariant with respect to the longitudinal boosts.

In practical, *i.e.* numerical, calculations of the invariant distribution given by Eqs. (11) and (13) a cut in the integral variable α_{\parallel} has to be done. So for the numerical reasons the range of α_{\parallel} is always finite and $-\alpha_{\parallel}^{cut} \leq \alpha_{\parallel} \leq \alpha_{\parallel}^{cut}$. The value of α_{\parallel}^{cut} is chosen in such a way that the remaining "tails" of the integral over α_{\parallel} are negligible. It has turned out that it is enough to put $\alpha_{\parallel}^{cut} = 3.0$ to determine the geometric parameters τ and ρ_{max} exact to four decimal places.

It should be reminded here that in this paper fits are done to the spectra measured at midrapidity ($y = 0$). Also the estimates for $dE_T/d\eta$ and $dN_{ch}/d\eta$ are done for $y = 0$. What is more, the values of α_{\parallel}^{max} predicted in Sec. IV C are greater than 3.0. Thus for the practical calculations at $y = 0$, the case with unlimited α_{\parallel} covers the case with the finite range of α_{\parallel} .

III. TRANSVERSE ENERGY AND CHARGED PARTICLE MULTIPLICITY DENSITIES

The experimentally measured transverse energy is defined as

$$E_T = \sum_{i=1}^L \hat{E}_i \cdot \sin \theta_i , \quad (16)$$

where θ_i is the polar angle, \hat{E}_i denotes $E_i - m_N$ (m_N means the nucleon mass) for baryons, $E_i + m_N$ for antibaryons and the total energy E_i for all other particles, and the sum is taken over all L emitted particles [16, 17].

The pseudorapidity density of particle species i is given by

$$\frac{dN_i}{d\eta} = \int d^2 p_T \frac{dy}{d\eta} \frac{dN_i}{d^2 p_T dy} = \int d^2 p_T \frac{p}{E_i} \frac{dN_i}{d^2 p_T dy} . \quad (17)$$

Analogously, the transverse energy pseudorapidity density for the same species can be written as

$$\frac{dE_{T,i}}{d\eta} = \int d^2 p_T \hat{E}_i \cdot \frac{p_T}{p} \frac{dy}{d\eta} \frac{dN_i}{d^2 p_T dy} = \int d^2 p_T p_T \frac{\hat{E}_i}{E_i} \frac{dN_i}{d^2 p_T dy} . \quad (18)$$

For the quantities at midrapidity one has (in the c.m.s., which is the RHIC case)

$$\frac{dN_i}{d\eta} \Big|_{mid} = \int d^2 p_T \frac{p_T}{m_T} \frac{dN_i}{d^2 p_T dy} , \quad (19)$$

$$\frac{dE_{T,i}}{d\eta} \Big|_{mid} = \begin{cases} \int d^2 p_T p_T \frac{m_T - m_N}{m_T} \frac{dN_i}{d^2 p_T dy} , & i = \text{baryon} \\ \int d^2 p_T p_T \frac{m_T + m_N}{m_T} \frac{dN_i}{d^2 p_T dy} , & i = \text{antibaryon} \\ \int d^2 p_T p_T \frac{dN_i}{d^2 p_T dy} , & i = \text{others} . \end{cases} \quad (20)$$

The overall charged particle and transverse energy densities can be expressed as

$$\frac{dN_{ch}}{d\eta} \Big|_{mid} = \sum_{i \in B} \frac{dN_i}{d\eta} \Big|_{mid} , \quad (21)$$

$$\frac{dE_T}{d\eta} \Big|_{mid} = \sum_{i \in A} \frac{dE_{T,i}}{d\eta} \Big|_{mid} , \quad (22)$$

where A and B ($B \subset A$) denote sets of species of finally detected particles, namely the set of charged particles $B = \{\pi^+, \pi^-, K^+, K^-, p, \bar{p}\}$, whereas A also includes photons, K_L^0 , n and \bar{n} [18].

IV. RESULTS

A. Determination of geometric parameters

Analyses of the particle ratios and p_T spectra at various centralities in the framework of the single freeze-out model were done for the preliminary RHIC data at $\sqrt{s_{NN}} = 200$ GeV [6, 7] in [5]. This approach proceeds in two steps. First, thermal parameters T and μ_B are fitted with the use of the experimental ratios of hadron multiplicities at midrapidity. It is assumed that these values are independent of the centrality. This is reasonable since the very weak centrality dependence of the particle ratios has been observed so far. Recent works of Ref. [19, 20, 21] have just confirmed this assumption. After then two next parameters, τ and ρ_{max} , are determined from the simultaneous fit

to the transverse-momentum spectra of π^\pm , K^\pm , p and \bar{p} . Both fits are performed with the help of the χ^2 method. Since the preliminary data for the p_T spectra [6, 7] differ from the final data [8, 9] and not all bins were fitted in [5], the fit procedure for determination of the geometric parameters of the model, τ and ρ_{max} , has been performed again for the purposes of this paper. Additionally, the PHENIX case at $\sqrt{s_{NN}} = 130$ GeV has been worked out once more, since the first published data were for three bins only [22]. The data for the next two bins, which were not fitted in [10], were added in the later report [23]. Also the BRAHMS spectra at various centralities for the measurement at $\sqrt{s_{NN}} = 200$ GeV [24] have not been fitted within the single-freeze-out model until now. The data points with $p_T > 3$ GeV have been excluded in the χ^2 analysis. The thermal parameters for the three cases of the maximal RHIC collision energy have been taken from the newer studies of the particle abundance ratios [20, 21]. According to these results, the thermal parameters are different for two experiments, PHENIX and STAR, in spite of the same collision energy. Fits to mostly PHENIX ratios gave the lower freeze-out temperature [20] than fits to STAR data only [21]. This observation has been confirmed in the present analysis: fits to the PHENIX spectra with substitution of the STAR freeze-out thermal parameters ($T = 160.0$ MeV and $\mu_B = 24.0$ MeV [21]) and fits to the STAR spectra with the use of the PHENIX freeze-out thermal parameters ($T = 155.2$ MeV and $\mu_B = 26.4$ MeV [20]) have proven to be much worse than the fits done within the same experiment and finally reported in this work (here "worse fit" means that its χ^2/NDF is greater). Also it has turned out that BRAHMS spectra fit better with the PHENIX thermal parameters. The older estimates of thermal parameters for RHIC at $\sqrt{s_{NN}} = 200$ GeV ($T = 165.6$ MeV and $\mu_B = 28.5$ MeV) given in Ref. [5] have proven to lead to fits to PHENIX spectra which are not statistically significant for all centralities, $\chi^2/NDF \geq 1.3$. It should be also mentioned at this point, that the values of thermal parameters ($T = 177$ MeV and $\mu_B = 29$ MeV) obtained in Ref. [26] result in fits which are much worse, $\chi^2/NDF \approx 3$.

The final results for the geometric parameters ρ_{max} and τ are gathered in Table I together with the corresponding values of χ^2/NDF for each centrality class additionally characterized by the number of participants N_{part} . Note that besides the most peripheral bins of the PHENIX measurements all fits are statistically significant. Other physical quantities like the surface velocity β_{\perp}^{max} , the volume at the beginning of the freeze-out $V_{f.o.}^{(1)}$, the maximal freeze-out time at the central slice $t_{f.o.}^{(2)}$ and the corresponding volume $V_{f.o.}^{(2)}$, which have been defined in Sec. II, are also given there. Note that values of ρ_{max} and τ fitted for the same spectra as in [10] (the 0 – 5%, 15 – 30% and 60 – 92% centrality bins for PHENIX at $\sqrt{s_{NN}} = 130$ GeV) are the same with 5% accuracy as given in [10], besides the peripheral bin. The model calculations take into account full feeding from weak decays besides the PHENIX case at $\sqrt{s_{NN}} = 200$ GeV where protons (antiprotons) from Λ ($\bar{\Lambda}$) decays are excluded. This needs some comments because the STAR Collaboration claims that its pion spectra are corrected for weak decays [9]. However, in the present analysis the best quality of the fit expressed by the value of χ^2/NDF in the STAR case is for full feeding from weak decays. Namely, if pions from Λ ($\bar{\Lambda}$) decays are subtracted then $\chi^2/NDF = 0.37$ for the 0 – 5% centrality bin, whereas if pions from all possible weak decays are excluded $\chi^2/NDF = 0.88$ for the same bin. With the full inclusion of pions from weak decays $\chi^2/NDF = 0.29$ (see Table I). That the single-freeze-out model with all the resonances and the full feeding from weak decays can fit the STAR spectra has been already noticed in [9] but, as it is stated there, with not satisfactory χ^2/NDF .

Values of the geometric parameters ρ_{max} and τ from Table I are presented in Figs. 1-3 as functions of N_{part} . Also there the lines of the best power approximations are depicted,

$$x \sim N_{part}^\kappa, \quad x = \rho_{max}, \quad x = \tau, \quad (23)$$

with a scaling exponent $\kappa = 0.40 - 0.43$ for ρ_{max} and $\kappa = 0.23 - 0.33$ for τ . Note that the scaling is almost ideal, only slight deviations can be observed for the most central bins in some cases (ρ_{max} and τ for PHENIX at $\sqrt{s_{NN}} = 200$ GeV, Fig. 1, and τ for PHENIX at $\sqrt{s_{NN}} = 130$ GeV, Fig. 3). Another interesting point would be to give at least a rough notion of what the predicted volumes $V_{f.o.}^{(1)}$ and $V_{f.o.}^{(2)}$ mean. The simplest way is to compare them with the volume of the colliding nucleus, which is the gold nucleus here. Since the volume of the gold nucleus at rest (V_{Au}) equals about 1160 fm 3 ($V_A = 4/3 \pi r_0^3 A$, $r_0 = 1.12$ fm), one can see that for the most central collisions at $\sqrt{s_{NN}} = 200$ GeV the volume at the beginning of the freeze-out, $V_{f.o.}^{(1)}$, is $\approx 3V_{Au}$, whereas the volume when the freeze-out ceases at the central slice, $V_{f.o.}^{(2)}$, equals $\approx 5V_{Au}$. For the most central bin at $\sqrt{s_{NN}} = 130$ GeV this is $\approx 1.9V_{Au}$ and $\approx 2.4V_{Au}$, respectively. As far as the lifespan of the system is considered the final moment of the freeze-out in the central slice, $t_{f.o.}^{(2)}$, has turned out to be about 10 fm for the most central bins. With the realistic assumption of the maximal possible value of the fluid rapidity, α_{\parallel}^{max} , which will be explored in Sec. IV C, and for values of α_{\parallel}^{max} obtained there, the moment when the freeze-out ceases entirely, $t_{f.o.}^{(3)}$, will be of the order of 10 $t_{f.o.}^{(2)}$, that is of the order of 100 fm for the most central collisions.

The extension of the model predictions for the invariant distributions to the low- p_T region (0.03-0.05 GeV for pions, 0.09-0.13 GeV for kaons and 0.14-0.21 GeV for protons and antiprotons) agree well with the available PHOBOS data

TABLE I: Values of the geometric parameters of the model for various centrality bins fitted with the use of the RHIC final data for the p_T spectra of identified charged hadrons [8, 9, 23, 24, 25]. Values of the thermal parameters are taken from the quoted references.

Collision case	Centrality [%]	N_{part}	ρ_{max} [fm]	τ [fm]	β_{\perp}^{max}	$V_{f.o.}^{(1)}$ [fm 3]	$t_{f.o.}^{(2)}$ [fm]	$V_{f.o.}^{(2)}$ [fm 3]	χ^2/NDF
PHENIX at $\sqrt{s_{NN}} = 130$ GeV:	0-5	347.7	6.50 ± 0.27	8.23 ± 0.23	0.62	2184.1	10.5	2782.2	0.52
	5-15	271.3	5.99 ± 0.21	7.29 ± 0.18	0.63	1641.1	9.4	2124.2	0.46
	15-30	180.2	5.08 ± 0.18	6.34 ± 0.15	0.63	1028.1	8.1	1317.6	0.49
$\mu_B = 41$ MeV	30-60	78.5	3.59 ± 0.15	4.81 ± 0.13	0.60	388.9	6.0	485.4	0.74
[2]	60-92	14.3	1.68 ± 0.19	3.14 ± 0.22	0.47	55.6	3.6	63.1	1.32
PHENIX at $\sqrt{s_{NN}} = 200$ GeV:	0-5	351.4	8.46 ± 0.10	8.84 ± 0.08	0.69	3973.4	12.2	5497.0	0.80
	5-10	299.0	7.99 ± 0.10	8.23 ± 0.08	0.70	3302.6	11.5	4602.9	0.61
	10-15	253.9	7.54 ± 0.10	7.67 ± 0.08	0.70	2736.2	10.8	3837.1	0.48
$\mu_B = 26.4$ MeV	15-20	215.3	7.11 ± 0.10	7.17 ± 0.07	0.70	2275.5	10.1	3203.0	0.48
[20]	20-30	166.6	6.45 ± 0.09	6.47 ± 0.07	0.71	1689.5	9.1	2386.3	0.58
	30-40	114.2	5.57 ± 0.08	5.63 ± 0.06	0.70	1097.2	7.9	1544.0	0.77
	40-50	74.4	4.68 ± 0.07	4.85 ± 0.06	0.69	669.0	6.7	929.8	1.05
	50-60	45.5	3.83 ± 0.07	4.16 ± 0.05	0.68	383.9	5.7	521.6	1.13
	60-70	25.7	2.99 ± 0.06	3.47 ± 0.05	0.65	194.3	4.6	256.5	1.41
	70-80	13.4	2.22 ± 0.06	2.78 ± 0.05	0.62	86.3	3.6	110.4	1.55
	80-92	6.3	1.71 ± 0.06	2.40 ± 0.05	0.58	44.2	2.9	54.2	1.40
STAR at $\sqrt{s_{NN}} = 200$ GeV:	0-5	352	9.22 ± 0.18	7.13 ± 0.06	0.79	3805.9	11.7	6222.1	0.29
	5-10	299	8.40 ± 0.17	6.83 ± 0.06	0.78	3029.0	10.8	4800.7	0.27
	10-20	234	7.57 ± 0.15	6.33 ± 0.06	0.77	2277.0	9.9	3548.3	0.23
$\mu_B = 24.0$ MeV	20-30	166	6.50 ± 0.14	5.86 ± 0.06	0.74	1557.9	8.8	2326.6	0.30
[21]	30-40	115	5.52 ± 0.12	5.37 ± 0.06	0.72	1028.9	7.7	1476.2	0.27
	40-50	76	4.66 ± 0.11	4.91 ± 0.06	0.69	669.8	6.8	922.7	0.27
	50-60	47	3.87 ± 0.10	4.40 ± 0.06	0.66	413.3	5.9	550.2	0.35
	60-70	27	3.07 ± 0.09	3.94 ± 0.06	0.61	232.9	5.0	295.3	0.46
	70-80	14	2.37 ± 0.08	3.32 ± 0.06	0.58	116.8	4.1	143.4	0.87
BRAHMS at $\sqrt{s_{NN}} = 200$ GeV:	0-5	357	8.75 ± 0.16	8.38 ± 0.11	0.72	4029.6	12.1	5825.3	0.50
	0-10	328	8.50 ± 0.15	8.08 ± 0.10	0.72	3670.6	11.7	5329.1	0.52
	10-20	239	7.52 ± 0.13	7.28 ± 0.09	0.72	2584.1	10.5	3714.1	0.46
$\mu_B = 26.4$ MeV	20-40	140	6.29 ± 0.12	6.20 ± 0.09	0.71	1541.5	8.8	2194.7	0.36
[20]	40-60	62	4.42 ± 0.12	4.95 ± 0.10	0.67	608.2	6.6	816.0	0.61

[28], even protons and antiprotons agree within errors as one can see in Fig. 4 (but the $\approx 30\%$ overestimation of protons and antiprotons has been obtained for the lowest p_T point of the PHENIX data, *i.e.* for $p_T = 0.65$ GeV). The similar result was obtained also for the preliminary data but protons and antiprotons were much more overweight [5]. In Fig. 4 the original PHENIX data [8] have been modified so as to be more useful for the comparison with the PHOBOS data [28]. Namely, the PHOBOS measurements were done for the 15% most central collisions whereas the PHENIX ones for the 0 – 5%, 5 – 10% and 10 – 15% centrality bins. Since the treatment of counts includes the averaging over the number of events in a given centrality bin and for the same run the number of events in the 15% most central bin should be equal to the sum of numbers of events in the 0 – 5%, 5 – 10% and 10 – 15% centrality bins, the rough approximation of the hypothetic measurement done in the 0 – 15% centrality bin would be the average of the measurements done in the 0 – 5%, 5 – 10% and 10 – 15% centrality bins. Therefore, in Fig. 4 the data points representing the PHENIX yields are such averages of the original values from [8]. The model predictions have been averaged in the same way.

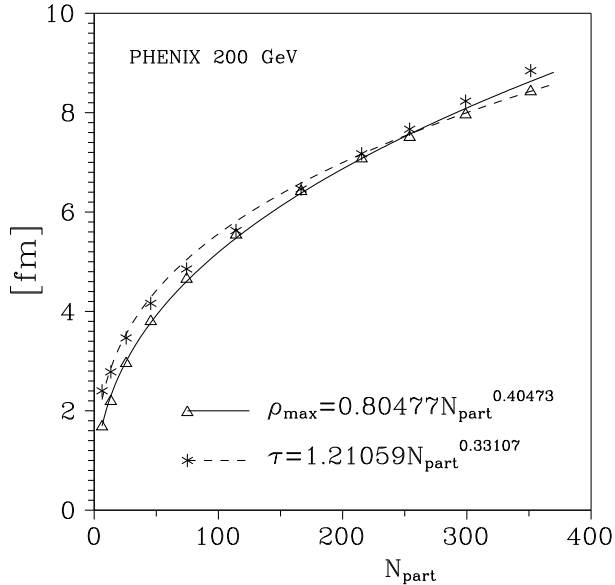


FIG. 1: Values of the geometric parameters of the model from the fourth and fifth column of Table I for PHENIX at $\sqrt{s_{NN}} = 200$ GeV. The lines are the best power approximations.

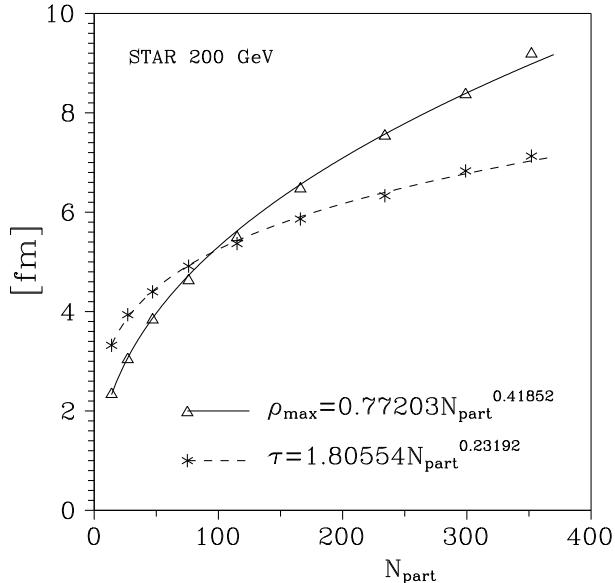


FIG. 2: Values of the geometric parameters of the model from the fourth and fifth column of Table I for STAR at $\sqrt{s_{NN}} = 200$ GeV. The lines are the best power approximations.

B. Estimations of transverse energy and charged particle multiplicity densities

The results of numerical estimations of $dN_{ch}/d\eta|_{mid}$ divided by the number of participant pairs for various centrality classes are presented in Figs. 5 and 6 for RHIC at $\sqrt{s_{NN}} = 130$ and 200 GeV, respectively. Additionally to the straightforward PHENIX measurements of the charged particle multiplicity density, also the data from the summing up of the integrated charged hadron yields [8, 23] are depicted in these figures (more precisely, since the integrated charged hadron yields are given as rapidity densities, the transformation to pseudo-rapidity should be done, which means the division by a factor 1.2 here, see [27]). Also in [8] the feeding of $p(\bar{p})$ from $\Lambda(\bar{\Lambda})$ decays is excluded. To diminish this effect, integrated p and \bar{p} yields delivered in [8] were corrected to include back the feeding. The correction was done by the division by a factor 0.65, which is the rough average of a p_T -dependent multiplier used

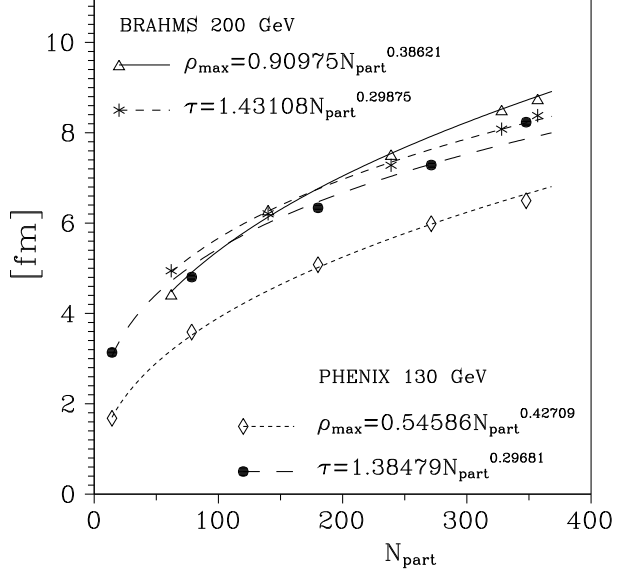


FIG. 3: Values of the geometric parameters of the model from the fourth and fifth column of Table I for BRAHMS at $\sqrt{s_{NN}} = 200$ GeV and PHENIX at $\sqrt{s_{NN}} = 130$ GeV. The lines are the best power approximations.

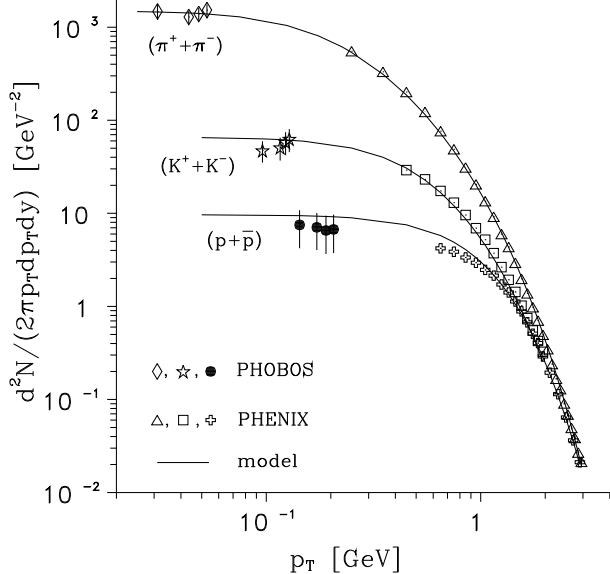


FIG. 4: Invariant yields as a function of p_T for RHIC at $\sqrt{s_{NN}} = 200$ GeV. The PHOBOS data are for the 15% most central collisions with the error bars expressed as the sum of the systematic and statistical uncertainties [28]. The corresponding PHENIX data are presented as the averages of the invariant yields for the 0 – 5%, 5 – 10% and 10 – 15% centrality bins with no errors given. Lines are the appropriate predictions of the single-freeze-out model.

by PHENIX Collaboration (see Fig.8 and Eq.(5) in [8]). Generally, the agreement of the model predictions with the data is much better for RHIC at $\sqrt{s_{NN}} = 200$ GeV. For the case of $\sqrt{s_{NN}} = 130$ GeV, only the qualitative agreement has been reached. The main reason of the $\approx 15\%$ underweight of $dN_{ch}/d\eta$ seen in Fig.5 is that the best fit estimates for the p_T spectra of pions at the lowest p_T lies 29% on the average below the corresponding measured values. This concerns also the PHENIX case at $\sqrt{s_{NN}} = 200$ GeV but the underestimation of low- p_T pions is smaller there (15% on the average). Since pions comprise about 80% of $dN_{ch}/d\eta$ and their low- p_T fraction can contribute even 30 % to the integrated yield [22], this explains the obtained underweight of $dN_{ch}/d\eta$ in spite of the very good quality of the fit for PHENIX at $\sqrt{s_{NN}} = 130$ GeV. The discrepancy between the directly measured dN_{ch}/dy and $dN_{ch}/d\eta$ expressed as the sum of the integrated charged hadron yields can be the next reason, especially for RHIC at $\sqrt{s_{NN}} = 200$ GeV

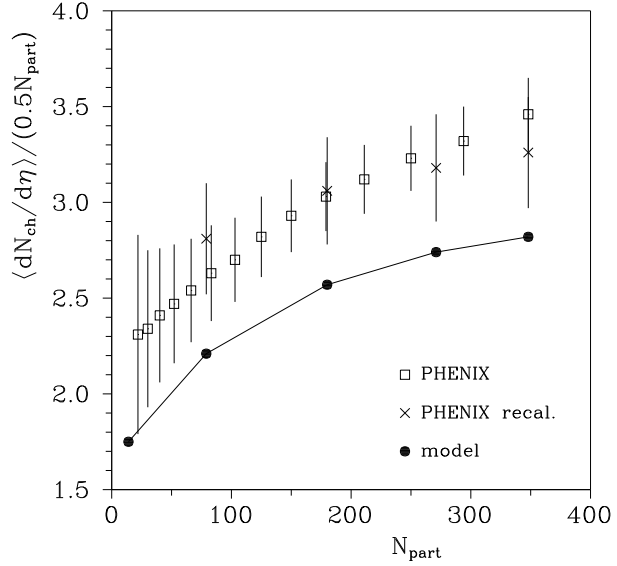


FIG. 5: $dN_{ch}/d\eta$ per pair of participants versus N_{part} for RHIC at $\sqrt{s_{NN}} = 130$ GeV. The PHENIX original data are from [17]. Also the recalculated PHENIX data from summing up the integrated charged hadron yields delivered in [23] are depicted. The line connects the results and is to guide the eye.

(see Fig. 6; this effect was notified in backup slides of [6]). The discrepancy starts at mid-centrality and rises with the centrality. The another reason for the quantitative disagreement is that transverse momentum spectra are measured in *limited ranges*, so very important low- p_T regions are not covered by the data. To obtain integrated yields some extrapolations below and above the measured ranges are used. In fact these extrapolations are only analytical fits, but contributions from regions covered by them account for about 25 – 40% of the integrated yields [22]. It might turned out that these extrapolations differ from the thermal distributions supplemented by the distributions of products of decays. However, the extension of the model predictions for the invariant distributions to the low- p_T region agree well with the available data, *cf.* Fig. 4.

The values of $dE_T/d\eta|_{mid}$ divided by the number of participant pairs are shown in Figs. 7 and 8 for $\sqrt{s_{NN}} = 130$ and 200 GeV, respectively. The quality of the model predictions for $dE_T/d\eta$ is much better then for $dN_{ch}/d\eta$. Again the worse agreement is for the case of $\sqrt{s_{NN}} = 130$ GeV. The STAR measurements need separate comments. The STAR data were taken not at mid-rapidity ($\eta = 0$) as in the PHENIX case but at $\eta = 0.5$ [16]. But the p_T spectra used for fits of the geometric parameters were measured at mid-rapidity, also in the STAR case [9]. Therefore one should expect some overestimation of the predictions in comparison with the data on the whole. To remove this effect the original STAR data [16] have been divided by a factor $\sin(\theta|_{\eta=0.5}) \approx 0.887$. As it can be seen from Fig. 8, the predictions and data agree with each other within errors besides two most central points. But even there, the discrepancy is $\approx 17\%$. It should be also noticed that bigger values of transverse energy estimates for the STAR case are the consequence of slightly higher values of p_T distributions measured by STAR Collaboration with respect to PHENIX measurements (it can be seen directly from careful comparison of spectra given in [9] and [8]).

Values of the ratio $\langle dE_T/d\eta \rangle / \langle dN_{ch}/d\eta \rangle$ as a function of N_{part} are presented in Figs. 9-11. As one can see, the position of model predictions is very regular and exactly resembles the configuration of the data in each case, the estimates are only shifted up about $\approx 10\%$ as a whole. For the PHENIX case, Figs. 9-10, the shift is about 8% at $\sqrt{s_{NN}} = 130$ GeV and about 14% at $\sqrt{s_{NN}} = 200$ GeV. This overestimation of the ratio can be explained, at least for more central collisions, by the observed discrepancy between the directly measured $dN_{ch}/d\eta$ and $dN_{ch}/d\eta$ expressed as the sum of the integrated charged hadron yields. If the original data points are replaced by the recalculated data, such that the denominators are sums of the integrated charged hadron yields, then much better agreement can be reached for more central collisions. In the STAR case, Fig. 11, as the experimental data at $\eta = 0$ two modified versions of the original data [16] at $\eta = 0.5$ are depicted. The first version was done by the division of the original data by a factor $\sin(\theta|_{\eta=0.5}) \approx 0.887$. In the second one, besides the above-mentioned rescaling, the values of $dN_{ch}/d\eta$ measured directly at $\eta = 0$ [9] were put into the denominator. Up to the mid-centrality the model estimates agree pretty well with the second version of the data, but for the most central bin the overestimation of the ratio of about 13% has been obtained.

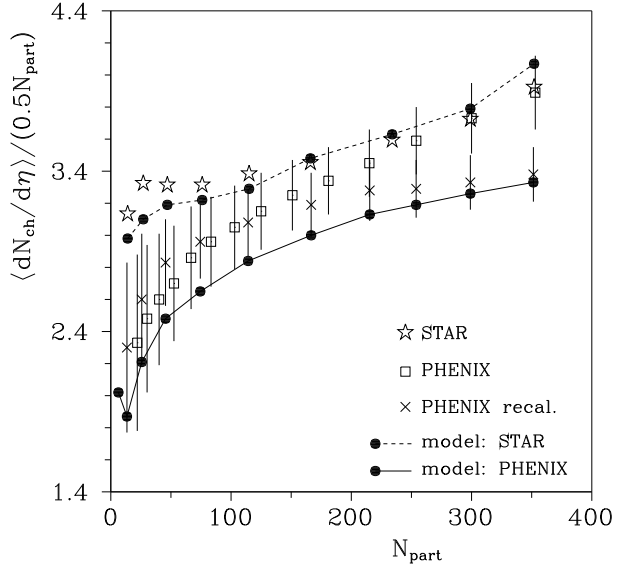


FIG. 6: $dN_{ch}/d\eta$ per pair of participants versus N_{part} for RHIC at $\sqrt{s_{NN}} = 200$ GeV. The original PHENIX data are from [17], whereas the recalculated PHENIX data are from summing up the integrated charged hadron yields delivered in [8]. Also the STAR data are depicted with no errors given as in the source paper [9]. The lines connect the results and are to guide the eye.

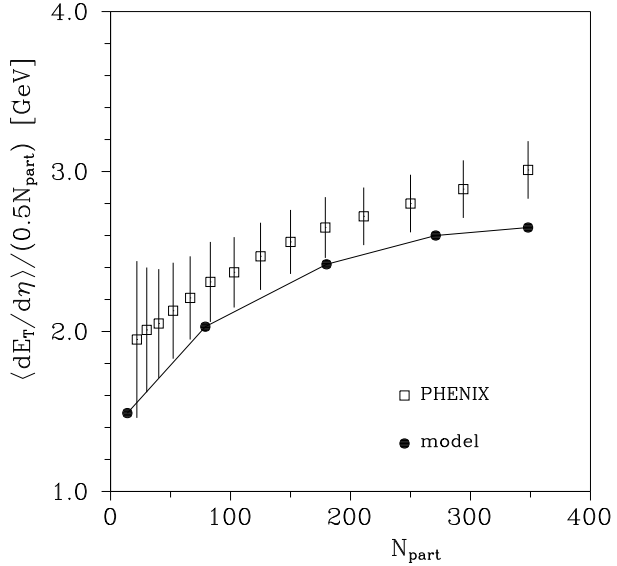


FIG. 7: $dE_T/d\eta$ per pair of participants versus N_{part} for RHIC at $\sqrt{s_{NN}} = 130$ GeV. The PHENIX data are from [17]. The line connects the results and is to guide the eye.

C. Total charged-particle multiplicity

Generally, for any expansion satisfying the condition $d\sigma_\mu \sim u_\mu$ on a freeze-out hypersurface, the total multiplicity of particle species i can be derived in the form (for the more formal proof see [10])

$$\begin{aligned}
 N_i &= \int d^2p_T dy \frac{dN_i}{d^2p_T dy} = \int d^2p_T dy \int p^\mu d\sigma_\mu f_i(p \cdot u) = \int d\sigma \int d^2p_T dy (p \cdot u) f_i(p \cdot u) \\
 &= \int d\sigma \int \frac{d^3\vec{p}}{E} (p \cdot u) f_i(p \cdot u) = \int d\sigma n_i(T, \mu_B) = n_i(T, \mu_B) \int d\sigma ,
 \end{aligned} \tag{24}$$

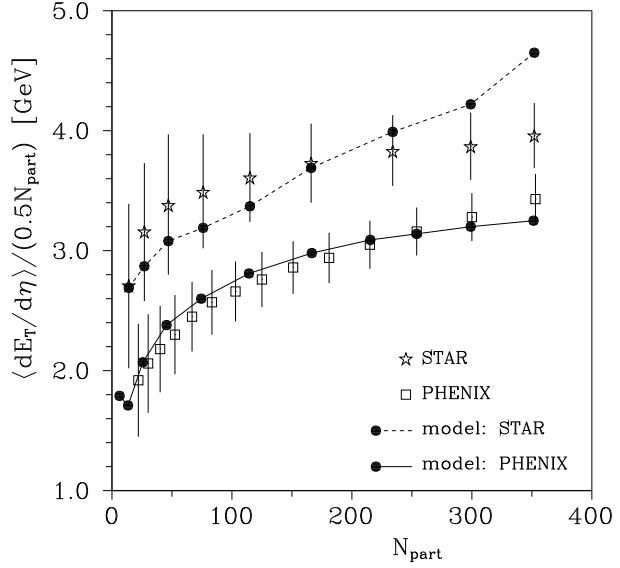


FIG. 8: $dE_T/d\eta$ per pair of participants versus N_{part} for RHIC at $\sqrt{s_{NN}} = 200$ GeV. The PHENIX data are from [17] but the original STAR data from [16] have been rescaled to $\eta = 0$, see text for more explanations). The lines connect the results and are to guide the eye.

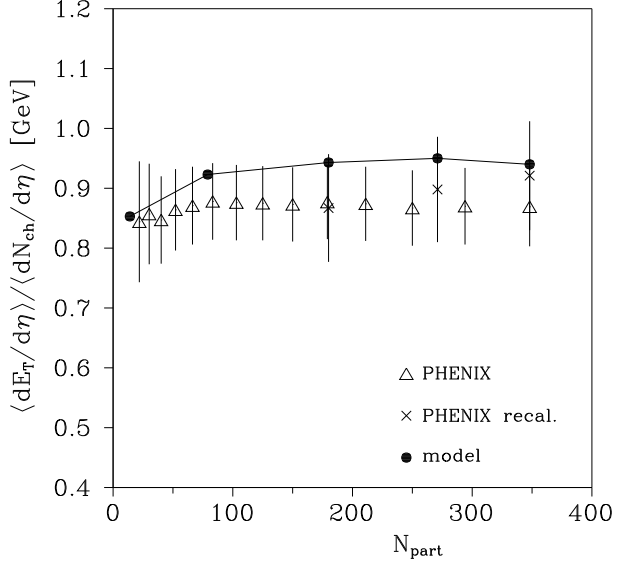


FIG. 9: $\langle dE_T/d\eta \rangle / \langle dN_{ch}/d\eta \rangle$ versus N_{part} for RHIC at $\sqrt{s_{NN}} = 130$ GeV. The original PHENIX data are from [17]. The recalculated PHENIX data are also depicted, here "recalculated" means that the sum of integrated charged hadron yields [22] have been substituted for the denominator in the ratio. The line connects the results and is to guide the eye.

if the local thermal parameters are constant on this hypersurface. This means that under such condition the total multiplicity is a product of the density n_i calculated for a static gas case and the hypersurface volume. Note that n_i is not the primordial thermal density of particle species i but it collects also contributions from decays of resonances. Since the freeze-out hypersurface and the flow described in Sec. II fulfill the condition $d\sigma_\mu \sim u_\mu$, the formula (24) is valid in this case as well. In practise the rapidity of the fluid element α_{\parallel} should not be unlimited but should have its maximal value α_{\parallel}^{max} . Otherwise, as it can be seen further, the hypersurface volume and the total charged particle multiplicity would be infinite. Then, with the use of Eq. (14) one can express the hypersurface volume as

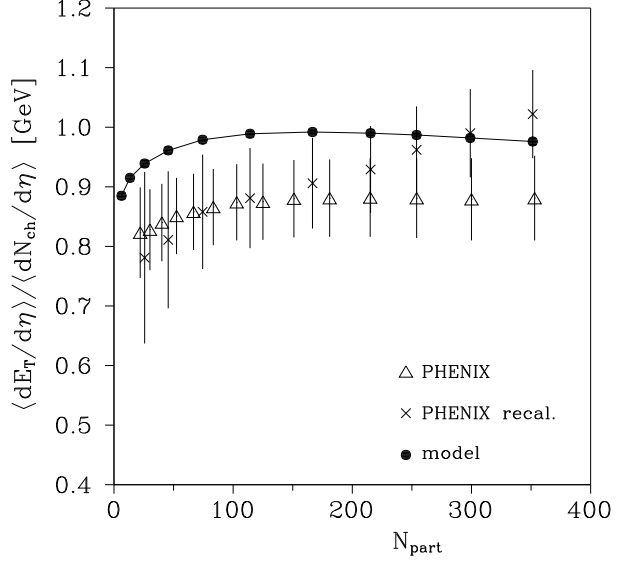


FIG. 10: $\langle dE_T/d\eta \rangle / \langle dN_{ch}/d\eta \rangle$ versus N_{part} for RHIC at $\sqrt{s_{NN}} = 200$ GeV. The original PHENIX data are from [17]. The recalculated PHENIX data are also depicted, here "recalculated" means that the sum of integrated charged hadron yields [8] have been substituted for the denominator in the ratio. The line connects the results and is to guide the eye.

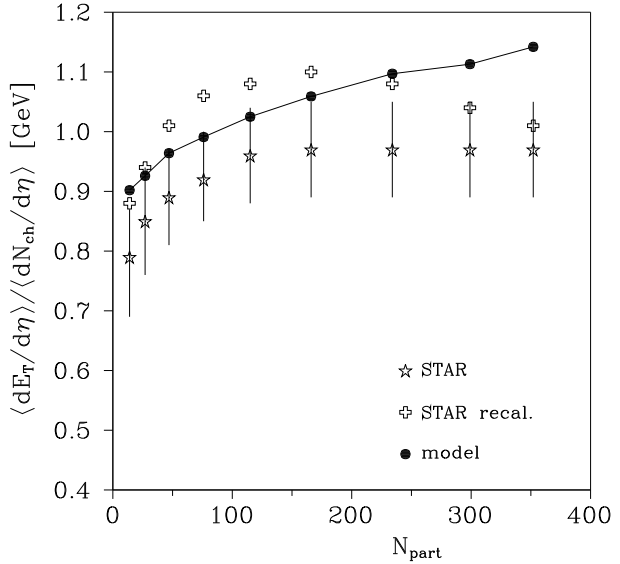


FIG. 11: $\langle dE_T/d\eta \rangle / \langle dN_{ch}/d\eta \rangle$ versus N_{part} for RHIC at $\sqrt{s_{NN}} = 200$ GeV. The original STAR data [16] have been rescaled to $\eta = 0$ by the division by a factor 0.887. Also the recalculated STAR data are depicted, here "recalculated" means that the original values of $dE_T/d\eta$ [16] have been divided by a factor 0.887 and values of $dN_{ch}/d\eta$ measured at midrapidity [9] are taken for the denominator, however errors are not given in [9]. The line connects the results and is to guide the eye.

$$\int d\sigma = \tau^3 \int_{-\alpha_{||}^{max}}^{+\alpha_{||}^{max}} d\alpha_{||} \int_0^{\rho_{max}/\tau} \sinh \alpha_{\perp} d(\sinh \alpha_{\perp}) \int_0^{2\pi} d\xi = 2\pi \alpha_{||}^{max} \tau \rho_{max}^2 . \quad (25)$$

Finally, the total multiplicity of charged particles can be obtained:

$$N_{ch} = 2\pi \alpha_{||}^{max} \tau \rho_{max}^2 \sum_{i \in B} n_i(T, \mu_B) = 2\pi \alpha_{||}^{max} \tau \rho_{max}^2 n_{ch}(T, \mu_B) . \quad (26)$$

One can see that the above formula has the form of the product of a volume and a density. This volume can be treated as an approximation of the size of the gas at the freeze-out (or an average volume of a hadron source). Approximation - because it is the volume of a static fireball which would emit the same amount of charged hadrons as the freeze-out hypersurface described by Eq. (1) with the superimposed limit in the range of α_{\parallel} . Average - because for the static fireball the freeze-out happens at a given moment of time, whereas in the discussed model the freeze-out extends in time. This approximate volume will be called $V_{stat.}$ from now on and equals

$$V_{stat.} = 2\pi \alpha_{\parallel}^{max} \tau \rho_{max}^2. \quad (27)$$

For α_{\parallel}^{max} the following reasonable assumption has been made: it is equal to the rapidity of leading baryons after the collision. In other words, it is assumed that the fluid which has been created in the CRR can not move faster in the longitudinal direction than fragments of a target or a projectile after the collision. Therefore it should depend on the centrality of the collision, since the more central the collision is, the higher degree of the stopping of the initial baryons ought to happen in principle. There are two limiting cases, the maximum stopping happens for the most central collision whereas if the centrality approaches 100% the stopping disappears. For values of α_{\parallel}^{max} it means that for the most central collision $\alpha_{\parallel}^{max} = \langle y \rangle = y_p - \langle \delta y \rangle$ and in the limiting case of the 100% centrality $\alpha_{\parallel}^{max} = y_p$, where $\langle y \rangle$ is the mean net-baryon rapidity after the collision, y_p the projectile rapidity and $\langle \delta y \rangle$ the average rapidity loss [25]. And the last assumption is that α_{\parallel}^{max} is a linear function of the centrality c , where c is a fractional number representing the middle of a given centrality bin, *i.e.* $c = 0.025$ for the 0–5% centrality bin, $c = 0.075$ for the 5–10% centrality bin, etc.. Then $\alpha_{\parallel}^{max}(c)$ has the following form:

$$\alpha_{\parallel}^{max}(c) = y_p - \frac{\langle \delta y \rangle}{0.975} \cdot (1 - c). \quad (28)$$

In the derivation of Eq. (28) the most central bin has been taken as the 0–5% centrality bin, since the estimate of the average rapidity loss $\langle \delta y \rangle$ for RHIC at $\sqrt{s_{NN}} = 200$ GeV was done for this centrality class in [25]. The BRAHMS Collaboration reports $\langle \delta y \rangle = 2.05$ for RHIC at $\sqrt{s_{NN}} = 200$ GeV ($y_p = 5.36$) [25]. Since for RHIC at $\sqrt{s_{NN}} = 130$ GeV the average rapidity loss has not been given yet, it is assumed that $\langle \delta y \rangle$ behaves linearly in y_p between the SPS point (the 5% most central Pb-Pb collision at 158 GeV per nucleon: $y_p = 2.9$ in the c.m.s. and $\langle \delta y \rangle = 1.76$ [29]) and the BRAHMS one. This results in $\langle \delta y \rangle = 2.0$ for RHIC at $\sqrt{s_{NN}} = 130$ GeV ($y_p = 4.93$). The numerical estimates of $n_{ch}(T, \mu_B)$ for the static gas give $n_{ch}(T = 155.2 \text{ MeV}, \mu_B = 26.4 \text{ MeV}) = 0.36112 \text{ fm}^{-3}$ and $n_{ch}(T = 160 \text{ MeV}, \mu_B = 24 \text{ MeV}) = 0.44839 \text{ fm}^{-3}$ for RHIC at $\sqrt{s_{NN}} = 200$ GeV and $n_{ch}(T = 165 \text{ MeV}, \mu_B = 41 \text{ MeV}) = 0.5618 \text{ fm}^{-3}$ for RHIC at $\sqrt{s_{NN}} = 130$ GeV. Now the total multiplicity of charged particles N_{ch} can be calculated with the use of Eqs. (26) and (28). The results presented as the total charged-particle multiplicity per participating pair versus N_{part} are gathered in Fig. 12. The predictions for STAR and PHENIX exhibit almost ideal centrality independence of the total charged-particle multiplicity per participating pair within the range of the PHOBOS measurement, *i.e.* $N_{part} \approx 60 - 360$. For the BRAHMS case there is some deviation from this ideal behavior, but it is of the order of 10%. Additionally, the predicted values agree with the data within $\approx 10\%$.

D. Comparison with the statistical hadronization model

Another very interesting point would be the comparison of the predictions of this model and the statistical hadronization model (SHM) of Ref. [20], from where values of the statistical parameters have been taken as an input to fit PHENIX and BRAHMS spectra at $\sqrt{s_{NN}} = 200$ GeV in Sec. IV A. An indirect comparison has been already done since good quality fits to the spectra have been obtained with the substitution of SHM statistical parameter estimates. This means that fits to the spectra with this model confirm values of statistical parameters obtained from fits to particle yields with SHM. The only left quantity which is independently obtained in these both models and could be directly compared is the volume of the hadron source. However not the global volume but the volume fraction dV/dy is predicted in [20]. The volume fraction is defined by the relation [30]:

$$\frac{dN_i}{dy} = \frac{dV}{dy} \cdot n_i, \quad (29)$$

which in principle should hold for each measured particle species i . Note that dN_i/dy depends on the centrality, so dV/dy does as well. According to Eq. (5) in [30] the volume of the hadron source is given by

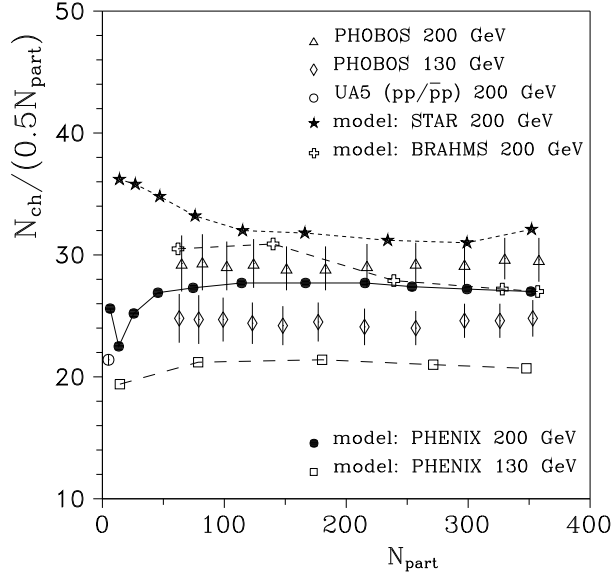


FIG. 12: N_{ch} per pair of participants versus N_{part} for RHIC at $\sqrt{s_{NN}} = 130$ and 200 GeV. The PHOBOS data are from [11] and the $pp/\bar{p}p$ data point of the UA5 measurement is from Fig.39.5 in [12]. The lines connect the results and are to guide the eye.

TABLE II: Comparison of predicted volumes of the hadron source for PHENIX at $\sqrt{s_{NN}} = 200$ GeV. Values of dV/dy are the SHM estimates taken from Ref. [20]. For all volumes the unit is cubic Femtometers.

Centrality [%]	N_{part}	$V_{stat.}$	V_{SHM}	dV/dy
0-5	351.4	13152	8233-12349	1920
5-10	299.0	11279	6899-10349	1609
10-15	253.9	9632	5694-8542	1328
15-20	215.3	8250	4961-7442	1157
20-30	166.6	6391	3666-5499	855
30-40	114.2	4381	2358-3538	550
40-50	74.4	2812	1466-2200	342

$$V_{SHM} = k \frac{dV}{dy} \cdot 2y_p , \quad (30)$$

where k is a constant, $k \simeq 0.4 - 0.6$ for RHIC and $2y_p$ expresses the maximum rapidity range. Since this volume is in fact the volume of a static fireball, the most natural volume appearing in the single freeze-out model which V_{SHM} can be compared with is $V_{stat.}$ - the static equivalent of the freeze-out volume, defined by Eq. (27). The detailed comparison of these both estimates of the volume of the hadron source for different centrality bins of PHENIX measurements at $\sqrt{s_{NN}} = 200$ GeV is given in Table II. One can see that values of $V_{stat.}$ and V_{SHM} agree with each other qualitatively. Some overestimation of $V_{stat.}$ with respect to V_{SHM} can be observed and this effect increases with the centrality. For the most central bin it is $\approx 6\%$ relative to the upper limit of the V_{SHM} range, whereas for the last listed one (40-50 %) the corresponding overestimation equals $\approx 28\%$.

V. CONCLUSIONS

The single freeze-out model has been applied to estimate transverse energy and charged particle multiplicity densities as well as the total multiplicity of charged particles for different centrality bins of RHIC measurements at $\sqrt{s_{NN}} = 130$ and 200 GeV. These three variables are independent observables, which means that they are measured independently of identified hadron spectroscopy. Since model fits were done to identified hadron data (particle yield ratios and p_T

spectra) and the global variables are calculable in the single freeze-out model, it was natural to check whether their estimated values agree with the data. Generally the answer is yes, at least on the qualitative level. This means that the similar shapes of the functional dependence on the centrality of the model predictions have been obtained, only their normalizations differ $\approx 10\%$ from the experimental data. In particular, the most surprising result is the almost ideal independence of the total charged-particle multiplicity per participating pair on the centrality of the collision in the range of centralities covered by the PHOBOS data [11]. The range is $N_{part} \approx 60 - 360$, that is from the bin around 50% centrality up to the most central one.

Even for $dN_{ch}/d\eta|_{mid}$ and $dE_T/d\eta|_{mid}$ this analysis is nontrivial and does not mean simply a self-consistency check of various measurements. First, transverse momentum spectra are measured in *limited ranges*, so very important low- p_T regions are not covered by the data. For instance, for PHENIX the lowest pion point is at $p_T = 0.25$ GeV/c, the lowest kaon one at $p_T = 0.45$ GeV/c and the proton and antiproton data start at $p_T = 0.65$ GeV/c [8, 22]. Therefore, to obtain integrated yields some extrapolations outside the measured ranges are used. In fact these extrapolations are only analytical fits without any physical reasoning, but, for instance, contributions from regions covered by them account for 30% of the yield for pions, 40% for kaons and 25% for protons and antiprotons for RHIC at $\sqrt{s_{NN}} = 130$ GeV [22]. On the other hand, a calorimeter acts very effectively for these species in the low- p_T range, namely pions with $p_T \leq 0.35$ GeV/c, kaons with $p_T \leq 0.64$ GeV/c and protons and antiprotons with $p_T \leq 0.94$ GeV/c deposit all their kinetic energy [18]. Second, it is impossible to check the consistency of the transverse energy data because not all stable hadron spectra are measured at midrapidity for each collision case. This mainly concerns neutrons and K_L^0 . Since the good predictions for the transverse energy density at midrapidity have been obtained (see Figs. 7-8), the present studies can be understood as an undirect proof that in these unmeasurable p_T regions spectra are also explicable by means of the thermal source with flow and decays. This has been also confirmed directly in the PHENIX case by the extension of the theoretical momentum distributions to the region of the very low transverse momentum covered by the PHOBOS detector (0.03-0.05 GeV for pions, 0.09-0.13 GeV for kaons and 0.14-0.21 GeV for protons and antiprotons), see Fig. 4.

Having compared the present results with the preliminary ones [1], one can notice that substantial improvement has been achieved for the PHENIX case at $\sqrt{s_{NN}} = 200$ GeV. In the previous analysis the behavior of the estimates of $dE_T/d\eta|_{mid}$ and $dN_{ch}/d\eta|_{mid}$ is very irregular in the region from peripheral to mid-central collisions and does not give the evidence for any clear dependence on the centrality. Here the dependence of predictions is exactly the same as the dependence of the data, only for $dN_{ch}/d\eta|_{mid}$ the underestimation of at most 15% has been obtained. But the main success of this final analysis is the prediction of the scaling of the total charged-particle multiplicity with the number of participants for all considered cases, which failed in the studies based on the preliminary fits from [5].

As the next point, the possible description of the HBT radii within the single-freeze-out model will be briefly discussed (for a general review of the HBT interferometry see, *e.g.*, [31]). This problem needs some comments since the HBT analysis also gives information about the size of the hadron source. Studies of the HBT radii in the single-freeze-out model have been already done for the PHENIX data at $\sqrt{s_{NN}} = 130$ GeV [32]. It has turned out that the values of the estimated radii are about 30 % smaller than the measured ones. This discrepancy has been improved by the introduction of the excluded-volume corrections for the hadron gas, in the way as postulated in Ref. [33]. The corrections give rise to the appearance of a new common scale factor, denoted as S^{-3} , in the invariant distribution, Eq. (11). This simply rescales both geometric parameters τ and ρ_{max} by the factor S , *i.e.* after fitting spectra τ/S and ρ_{max}/S have the same values as τ and ρ_{max} obtained for the point-like gas and listed in Table I. The value $S = 1.3$ has been found in Ref. [32] what implies the increase of τ and ρ_{max} by 30 %. With these new rescaled parameters the predicted values of the HBT radii agree fairly well with the data [32]. Of course the detailed analysis of the HBT radii in the context of the single-freeze-out model for the final RHIC data at $\sqrt{s_{NN}} = 200$ GeV should be performed and this will be the subject of further investigations.

Finally, it should be notice that the statistical model of the present analysis corresponds to the chemical equilibrium case of the more general statistical hadronization model applied in Ref. [20] (for a comprehensive review of the model see [34]). In some sense this analysis is complementary to those studies, because the estimates of statistical parameters from there have been taken as the input here and good quality fits have been obtained. Also the qualitative agreement between independent estimates of the volume of the hadron source done in both works has been obtained, *cf.* Table II. But as it was shown in Ref. [20], the assumption of the strange quark non-equilibrium and further also the light quark non-equilibrium leads to more thorough description of particle yields for all accessible centralities of PHENIX measurements at $\sqrt{s_{NN}} = 200$ GeV. Therefore such generalization of the present model should be done and tested with the data and this will be the subject of the next publication.

To summarize, the single freeze-out version of a statistical (equilibrium) model fairly well explains the measured spectra of identified hadrons for various centralities and the centrality dependence of transverse energy and charged particle multiplicity pseudo-rapidity densities at mid-rapidity observed at RHIC. The fact which should be stressed again is that this model predicts the centrality independence of the total charged-particle multiplicity. Also predicted values of the total charged-particle multiplicity per participating pair agree with the measured ones within $\approx 10\%$.

This is remarkable since geometric parameters have been fitted to spectra measured at *midrapidity* but the total charged-particle multiplicity deals with *the whole rapidity range*.

Acknowledgments

The author would like to thank Jan Rafelski for very helpful comments. This work was supported in part by the Polish Committee for Scientific Research under Contract No. KBN 2 P03B 069 25.

[1] D. Prorok, Eur. Phys. J. A **26**, 277 (2005).
 [2] W. Florkowski, W. Broniowski and M. Michalec, Acta Phys. Polon. B **33**, 761 (2002).
 [3] W. Broniowski and W. Florkowski, Phys. Rev. Lett. **87**, 272302 (2001).
 [4] W. Broniowski and W. Florkowski, Phys. Rev. C **65**, 064905 (2002).
 [5] A. Baran, W. Broniowski and W. Florkowski, Acta Phys. Polon. B **35**, 779 (2004).
 [6] T. Chujo [PHENIX Collaboration], Nucl. Phys. A **715**, 151 (2003) and
<http://alice-france.in2p3.fr/qm2002/Transparencies/20Plenary/Chujo.ppt>.
 [7] O. Barannikova and F. Wang [STAR Collaboration], Nucl. Phys. A **715**, 458 (2003).
 [8] S. S. Adler *et al.* [PHENIX Collaboration], Phys. Rev. C **69**, 034909 (2004).
 [9] J. Adams *et al.* [STAR Collaboration], Phys. Rev. Lett. **92**, 112301 (2004).
 [10] W. Broniowski, A. Baran and W. Florkowski, Acta Phys. Polon. B **33**, 4235 (2002).
 [11] B. B. Back *et al.* [PHOBOS Collaboration], arXiv:nucl-ex/0301017.
 [12] K. Hagiwara *et al.* [Particle Data Group Collaboration], Phys. Rev. D **66**, 010001 (2002).
 [13] M. Csanad, T. Csorgo, B. Lorstad and A. Ster, J. Phys. G **30**, S1079 (2004).
 [14] M. Chojnacki, W. Florkowski and T. Csorgo, Phys. Rev. C **71**, 044902 (2005).
 [15] D. Prorok, Eur. Phys. J. A **24**, 93 (2005).
 [16] J. Adams *et al.* [STAR Collaboration], Phys. Rev. C **70**, 054907 (2004).
 [17] S. S. Adler *et al.* [PHENIX Collaboration], Phys. Rev. C **71**, 034908 (2005) [Erratum-ibid. C **71**, 049901 (2005)].
 [18] K. Adcox *et al.* [PHENIX Collaboration], Phys. Rev. Lett. **87**, 052301 (2001).
 [19] J. Cleymans, B. Kampfer, M. Kaneta, S. Wheaton and N. Xu, Phys. Rev. C **71**, 054901 (2005).
 [20] J. Rafelski, J. Letessier and G. Torrieri, Phys. Rev. C **72**, 024905 (2005).
 [21] O. Barannikova [STAR Collaboration], J. Phys. G **31**, S93 (2005).
 [22] K. Adcox *et al.* [PHENIX Collaboration], Phys. Rev. Lett. **88**, 242301 (2002).
 [23] K. Adcox *et al.* [PHENIX Collaboration], Phys. Rev. C **69**, 024904 (2004).
 [24] I. Arsene *et al.* [BRAHMS Collaboration], Phys. Rev. C **72**, 014908 (2005).
 [25] I. G. Bearden *et al.* [BRAHMS Collaboration], Phys. Rev. Lett. **93**, 102301 (2004).
 [26] P. Braun-Munzinger, K. Redlich and J. Stachel, in *Quark-Gluon Plasma 3*, eds R. C. Hwa and Xin-Nian Wang (World Scientific Publishing, Singapore, 2004), p. 491.
 [27] A. Bazilevsky [PHENIX Collaboration], Nucl. Phys. A **715**, 486 (2003).
 [28] B. B. Back *et al.* [PHOBOS Collaboration], Phys. Rev. C **70**, 051901(R) (2004).
 [29] H. Appelshauser *et al.* [NA49 Collaboration], Phys. Rev. Lett. **82**, 2471 (1999).
 [30] J. Letessier and J. Rafelski, arXiv:nucl-th/0504028.
 [31] G. Baym, Acta Phys. Polon. B **29**, 1839 (1998).
 [32] W. Broniowski, A. Baran and W. Florkowski, AIP Conf. Proc. **660**, 185 (2003).
 [33] G. D. Yen, M. I. Gorenstein, W. Greiner and S. N. Yang, Phys. Rev. C **56**, 2210 (1997).
 [34] J. Letessier and J. Rafelski, Cambridge Monogr. Part. Phys. Nucl. Phys. Cosmol. **18** 1 (2002).